PLOS ONE

RESEARCH ARTICLE

Small molecule allosteric inhibitors of RORγt block Th17-dependent inflammation and associated gene expression *in vivo*

Steven A. Saenz[1]*, Andrea Local[2], Tiffany Carr[1], Arvind Shakya[2], Shivsmriti Koul[2], Haiqing Hu[3], Lisa Chourb[3], Justin Stedman[3], Jenna Malley[4¤a], Laura Akullian D'Agostino[5], Veerabahu Shanmugasundaram[5], John Malona[6¤b], C. Eric Schwartz[6¤c], Lisa Beebe[3], Meghan Clements[4¤d], Ganesh Rajaraman[4¤e], John Cho[7¤f], Lan Jiang[1], Alex Dubrovskiy[1], Matt Kreilein[8], Roman Shimanovich[3], Lawrence G. Hamann[5¤a], Laure Escoubet[2], J. Michael Ellis[5]*

1 Immunology, Cardiovascular & Fibrosis, Bristol Myers Squibb, Cambridge, Massachusetts, United States of America, 2 Oncogenesis Thematic Research Center, Bristol Myers Squibb, San Diego, California, United States of America, 3 Preclinical Candidate Optimization, Bristol Myers Squibb, Cambridge, Massachusetts, United States of America, 4 Nonclinical Development, Celgene Corporation, Cambridge, Massachusetts, United States of America, 5 Small Molecule Drug Discovery, Bristol Myers Squibb, Cambridge, Massachusetts, United States of America, 6 Drug Substance Development, Bristol Myers Squibb, Summit, New Jersey, United States of America, 7 Immunology & Inflammation, Celgene Corporation, Cambridge, Massachusetts, United States of America, 8 Drug Substance Development, Bristol Myers Squibb, Summit, New Jersey, United States of America

¤a Current address: Takeda Pharmaceuticals, Cambridge, Massachusetts, United States of America
¤b Current address: Jnana Therapeutics, Boston, Massachusetts, United States of America
¤c Current address: Cedilla Therapeutics, Cambridge, Massachusetts, United States of America
¤d Current address: AbbVie, Worcester, Massachusetts, United States of America
¤e Current address: Novartis Pharmaceuticals, Cambridge, Massachusetts, United States of America
¤f Current address: KSQ Therapeutics, Cambridge, Massachusetts, United States of America
* steven.saenz@bms.com (SAS); michael.ellis@bms.com (JME)

OPEN ACCESS

Data Availability Statement: All relevant data are within the manuscript and its Supporting Information files.

Abstract

Retinoic acid receptor-related orphan nuclear receptor (ROR) γt is a member of the RORC nuclear hormone receptor family of transcription factors. RORγt functions as a critical regulator of thymopoiesis and immune responses. RORγt is expressed in multiple immune cell populations including Th17 cells, where its primary function is regulation of immune responses to bacteria and fungi through IL-17A production. However, excessive IL-17A production has been linked to numerous autoimmune diseases. Moreover, Th17 cells have been shown to elicit both pro- and anti-tumor effects. Thus, modulation of the RORγt/IL-17A axis may represent an attractive therapeutic target for the treatment of autoimmune disorders and some cancers. Herein we report the design, synthesis and characterization of three selective allosteric RORγt inhibitors in preclinical models of inflammation and tumor growth. We demonstrate that these compounds can inhibit Th17 differentiation and maintenance *in vitro* and Th17-dependent inflammation and associated gene expression *in vivo*, in a dose-dependent manner. Finally, RORγt inhibitors were assessed for efficacy against tumor formation. While, RORγt inhibitors were shown to inhibit tumor formation in pancreatic ductal adenocarcinoma (PDAC) organoids *in vitro* and modulate RORγt target genes *in*

vivo, this activity was not sufficient to delay tumor volume in a KP/C human tumor mouse model of pancreatic cancer.

Introduction

Psoriasis is a chronic, immune-mediated disease characterized by the presence of large, erythematous, scaly plaques commonly found at multiple sites on the skin surface [1–3]. Psoriatic skin lesions display increased infiltrates of multiple lymphocyte lineages, including T helper type 17 (Th17) cells, γδT cells and innate lymphoid cells (ILCs), in the epidermal and dermal layers [3]. In addition, elevated gene expression levels of proinflammatory cytokines including TNFα, IL-17A, IL-22 and IL-23 have been reported in skin biopsies from psoriatic patients [2–4]. These cytokines are known to act on various cell types within the skin tissue microenvironment, including keratinocytes, neutrophils, endothelial cells and fibroblasts which, in turn, promote aberrant keratinocyte activation, hyperproliferation and tissue inflammation. For patients with moderate-to-severe psoriasis, treatment options are limited. Phototherapy or systemic medications including methotrexate and cyclosporine are common, as are neutralizing monoclonal antibodies against TNFα. However, these therapies are not broadly efficacious.

Retinoic acid receptor-related orphan nuclear receptor c (RORC) is a nuclear hormone receptor in the retinoid acid receptor-related orphan receptor (ROR) subfamily of transcription factors including two isoforms that vary at the N-Terminus [5]. RORγ is widely expressed while RORγt is induced during the transition from double negative to double positive thymocytes where it regulates the survival factor Bcl-xL, allowing for maturation into single positive T cells [5, 6]. Beyond its role in thymopoiesis, RORγt is expressed in subsets of immune cells including γδT cells, Th17 cells, ILC3, NKT cells and NK cells [5]. RORγt is the master regulator of Th17 cells. In response to IL-1α/β, IL-6 and IL-23, it regulates differentiation of Th17 cells as well as maintenance and production of cytokines including: IL-17A, IL-17F, IL-22 and granulocyte-macrophage colony stimulating factor (GM-CSF) [7, 8]. The primary function of Th17 cells is to regulate immune responses that lead to clearance of extracellular pathogens including bacteria and fungi. However, excessive IL-17A production has been linked to autoimmune diseases such as psoriasis, psoriatic arthritis, rheumatoid arthritis and multiple sclerosis [9]. Thus, the discovery that RORγt regulates the development of multiple lymphocyte lineages including IL-17A-producing immune cell populations provides compelling evidence that disruption of the RORγt/IL-17A/IL-23 axis may represent a viable therapeutic option for the treatment of psoriasis.

Targeting the RORγt/IL-17A/IL-23 axis, either by genetic manipulation or antibody-mediated neutralization of pathway cytokines (e.g. IL-17A, IL-23 and GM-CSF) ameliorates disease pathology in multiple animal models of autoimmunity and inflammation. These findings extend to patients, where biologic therapies targeting IL-23 and IL-17A or their receptors have demonstrated clinical efficacy in psoriasis, psoriatic arthritis, autoimmune uveitis and ankylosing spondylitis. In addition, small molecules targeting the RORγt/IL-17A/IL-23 axis have demonstrated clinical efficacy through reduction in circulating IL-17A levels. In multiple phase 3 trials in psoriasis patients, Otezla (Apremilast), a phosphodiesterase 4 (PDE4) inhibitor, reduced the production of IL-17A, IL-17F, IL-22 and TNFα by 40–50% at Week 4 with concomitant Psoriasis Area and Severity Index (PASI) -75 response rates of approximately 30% at Week 16 [10]. Furthermore, VTP-43742, an orthosteric RORγt modulator, demonstrated 50–75% reductions in IL-17A and IL-17F levels in the plasma of plaque psoriasis patients with 25–

30% PASI-75 response rates at Week 4 [11]. These data demonstrate that small molecule inhibitors targeting RORγt can block Th17-associated protein production across multiple cell populations with improved clinical outcomes.

As a key regulator of CD4^{+} T-cell polarization and Th17 cell function, RORγt is thought to play a key role in tumor immunity [12, 13]. In fact, knockout of RORγt in adult mice leads to development of lymphoblastic lymphomas within 6 months in a manner similar to embryonic RORγt loss [14]. RORγt agonists are currently in clinical trials for multiple indications including NSCLC and ovarian cancer [15]. However, as Th17 cells have been ascribed both pro- and anti-tumor effects, based on disease type and presence of other immune cells and cytokines, the role of RORγt in tumor immunity is controversial [12]. A recent study demonstrated that advanced or metastatic pancreatic tumors had increased RORγt expression. The study utilized transcriptomic and epigenetic profiling of a pancreatic ductal carcinoma (PDAC) KP/C mouse model to identify transcription factors important for cancer stem cell (CSC) maintenance and growth [16]. PDAC CSCs are known to be resistant to cytotoxic therapies like standard of care gemcitabine, and higher CSC levels are associated with decreased survival [17]. The contribution of several transcription factors to tumor cell growth, including RORγt, was confirmed using CRISPR knockout screens in mouse PDAC organoid models. Furthermore, it was demonstrated that genetic ablation of RORγt or modulation of its activity by SR2211, was sufficient to inhibit both human and mouse xenograft tumor growth [16].

Given the level of clinical validation for targeting the RORγt/IL-17A/IL-23 pathway, our aim was to evaluate additional allosteric inhibitors, complementary to previously reported ROR inhibitors [18, 19], in relevant pre-clinical assays to identify a suitable candidate for further drug development. Herein we detail the design, synthesis and pre-clinical characterization of three selective allosteric RORγt inhibitors, Compounds **1**, **2** and **3**, in models of inflammation and tumor growth. Potencies of these compounds were determined using GAL4 reporter assays and human primary cell Th17 differentiation and maintenance assays. Relationships between pharmacokinetics and pharmacodynamics (PK/PD) were established by monitoring Th17-associated gene expression after dosing in Th17-dependent mouse models of imiquimod-induced skin inflammation and experimental autoimmune encephalitis (EAE). Finally, the antitumor activity of Compound **3** was assessed in PDAC organoids and the genetically engineered KP/C mouse model.

Materials and methods

Crystallization, data collection and structure determination

A single crystal of Compound **3** was successfully grown by Wilmington PharmaTech (Newark, DE, USA) in acetonitrile and the structure was analyzed by single-crystal x-ray diffraction. Compound **3** was dissolved in acetonitrile (1.0mL) in a 4 mL vial and stored in hood 23–25°C for 6 days, at which point flat-shaped crystals were observed. Single crystal X-ray diffraction was obtained on the sample. The results indicated only the (*R*,*R*)-enantiomer is present in the crystal sample, which is a hemihydrate with two symmetry unique compound molecules per water molecule. The H atoms on oxygen atoms were located and they appear to have normal H-bonding interactions. Each CF_3 group is disordered with a Cl group but the disorder has been modeled. A specimen of $C_{22}H_{16}ClF_4N_2O_{4.5}$ approximate dimensions 0.046 mm x 0.40 mm x 0.456 mm, was used for the X-ray crystallographic analysis. The X-ray intensity data were measured.

The total exposure time was 21.67 hours. The frames were integrated with the Bruker SAINT software package using a narrow-frame algorithm. The integration of the data using a triclinic unit cell yielded a total of 20622 reflections to a maximum θ angle of 27.66° (0.77 Å

resolution), of which 10005 were independent (average redundancy 2.061, complete-ness = 99.8%, R_{int} = 1.94%, R_{sig} = 3.07%) and 8845 (88.41%) were greater than $2\sigma(F^2)$. The final cell constants of $\underline{a}$ = 7.2225(12) Å, $\underline{b}$ = 7.6694(12) Å, $\underline{c}$ = 21.269(3) Å, α = 82.420(2˚, β = 85.842(2˚, γ = 67.344(2˚, volume = 1077.4(3) Å^3, are based upon the refinement of the XYZ-centroids of 8667 reflections above 20 σ(I) with 5.793˚ < 2θ < 54.41˚. Data were corrected for absorption effects using the Multi-Scan method (SADABS). The ratio of minimum to maximum apparent transmission was 0.933. The calculated minimum and maximum transmission coefficients (based on crystal size) are 0.8960 and 0.9890.

The structure was solved and refined using the Bruker SHELXTL Software Package, using the space group P 1, with Z = 2 for the formula unit, C22H16ClF4N2O4.50. The final aniso-tropic full-matrix least-squares refinement on F2 with 696 variables converged at R1 = 3.83%, for the observed data and wR2 = 9.41% for all data. The goodness-of-fit was 1.065. The largest peak in the final difference electron density synthesis was 0.385 e-/Å3 and the largest hole was -0.269 e-/Å3 with an RMS deviation of 0.040 e-/Å3. On the basis of the final model, the calcu-lated density was 1.516 g/cm3 and F(000), 502 e-.

The small molecule crystal structure coordinates have been deposited with the Cambridge Crystallographic Data Centre (CCDC) and the coordinates will be released upon publication. Compound ID Number: 2065542. The CIF file and check CIF validation report are provided as supporting information.

Mice & imiquimod (IMQ)-induced skin inflammation & experimental autoimmune encephalomyelitis (EAE) model

For IMQ-induced skin inflammation, wild-type (WT) Balb/c female mice, 5–8 weeks of age, were purchased from Charles River Laboratories. All mice were housed in pathogen-free con-ditions at Bristol Myers Squibb (Cambridge, MA). Aldara cream containing 5% imiquimod (Patterson Veterinary Supply, Inc; Devens, MA) was applied to the ears daily (11–14 mg) for 3 days. Mice were treated twice daily (BID) on days 1–4 per os (PO) with vehicle (0.5% methyl-cellulose/0.25% Tween80) or RORγt inhibitors at indicated doses immediately prior to Aldara application. Ear thickness was measured using micro-calipers. Tissues were harvested on day 4, 2 hours following the last compound dose. Naïve mice are completely untreated, receiving neither control vehicle for IMQ nor Compound.

EAE studies were conducted at Hooke Laboratories. WT female C57BL/6 mice (Taconic Labs) 9 weeks of age were inoculated on day 0 with MOG_{35-55} peptide (Hooke Kit™ MOG35-55/CFA Emulsion PTX) (EK-2110, Hooke Laboratories, Lawrence MA) followed by intraperi-toneal (IP) injections of pertussis toxin at 2 and 24 hours. Mice were treated twice daily (BID, starting at day 1) per os (PO) with vehicle (0.5% MC/0.25% Tween80) or RORγt inhibitors at indicated doses. FTY720 (Gilenya) was dosed once daily (QD) at 3 mg/kg starting at day 1. EAE clinical scores were evaluated daily and scored from 0–5 according to Hooke Lab EAE scoring guidelines http://hookelabs.com/services/cro/eae/MouseEAEscoring.html. Mean clini-cal scores & body weight loss were assessed and statistical significance calculated by Wilcox-on's non-parametric or 2-tailed Student's t-test, respectively. All studies performed were approved in accordance with the Institutional Animal Care and Use Committee of Bristol Myers Squibb and complied according to Bristol Myers Squibb guidelines.

In vivo tumor growth suppression

Pancreatic tumor chunks from KP/C mice [20] on C57Bl/6 background were inoculated sub-cutaneously in the flank of syngeneic mice. Mice were randomized and distributed in 5 groups of 8 mice each with an average tumor volume of 100 mm^3. Mice were treated with Compound

3 (30mg/kg, BID), Gemcitabine (120mg/kg, QW) or Cisplatin (5mg/kg, QW). Tumor volumes and body weight were measured twice each week.

Pancreatic organoid cell culture

Patient derived organoids were established as previously described [21]. Briefly, PDX tumor chunks were minced then enzymatically digested into single cells by using a tumor dissociation Kit (Miltenyi, Cat# 130-095-929). Mouse and human cells were separated through magnetic separation, and isolated tumor cells were cultured on Matrigel-coated dishes. Organoid cultures were maintained by growing on Matrigel in human complete maintenance media: Advanced DMEM/F12 media (Life Technology, Cat# 12634028), 10 mM HEPES (Life Technology, Cat# 15630–080), 1X Glutamax (Life Technology, Cat# 35050–061), 1X Antibiotic-Antimycotic (Life Technology, Cat# 15240–062), 10 mM Nicotinamide (Sigma-Aldrich, Cat# N0636-500G), 250 ng/mL R-Spondin-1 (Peprotech, Cat# 120–38), 100 ng/mL Noggin (Peprotech, Cat# 120-10C), 50 ng/mL EGF (Peprotech, Cat# AF-100-15), 100 ng/mL FGF10 (Peprotech, Cat# 100–26), 10 mM Gastrin-1 (Sigma-Aldrich, Cat# G9020), 500 nM A83-01 (Sigma, Cat# SML0788), 20 μM Y-27632 (LC Laboratories, Cat# Y-5301), 1X B27 (Life Technology, Cat# 12587010), 10 ng/mL Wnt3a (R&D Systems, Cat# 5036-WN-010), 0.1% Methylcelluose (R&D Systems, Cat# HSC001) and Plasmocin (Invivogen, Cat# Ant-mpp) and were passaged every 10–14 days. Organoids were isolated from Matrigel (Corning, Cat# 08-774-406) in a cell recovery solution (Corning, Cat# CB-40253). Spheroid clusters were then dissociated into a single cell suspension with TrypLE (Gibco, Cat# 12605). After dissociation, single cells were suspended in the complete growth medium as described above. After counting, a single-cell organoid suspension was plated on pre-warmed matrigel coated plates.

In vitro organoid growth assay

Organoids were isolated and dissociated as described above. Cell numbers were counted by trypan blue exclusion and 5000 cells per well were plated on the Matrigel coated and pre-warmed 96-well plates. Compound **3** and SR2211 (**4**) were prepared in DMSO to a stock concentration of 10 μM and were added in indicated doses (0.03 μM to 30 μM) either on the first day or third day of plating. 100 μl of CellTiter-Glo® 3D reagent (Promega cat# G9682) was added to each well after desired time points and luminescence signal measured after 30 minutes.

RNA collection, gene expression, cytokine production analysis

For RNA isolation & gene expression, ears are collected on day 4 in RNAlater (Qiagen) and stored at 4˚C until processed. Ears were homogenized using Procellys 24 homogenizer & hard tissue homogenizing beads (Bertin Instruments), 2 cycles of 30 seconds @ 6000 rpm in RLT lysis buffer according to manufacturer's instructions. RNA was isolated using RNAeasy Plus MiniPrep columns (Qiagen) and cDNA generated using SuperScript VILO cDNA Synthesis kit (Invitrogen). Gene expression was quantified using TaqMan Fast Master Mix & and TaqMan FAM-MGB probe sets (Applied Biosystems): *Gapdh*, Mm99999915_g1, *Il17a*, Mm00439618_m1, *Il17f*, Mm00521423_m1, Il22, Mm01226722_g1 & Bclxl, Mm00437783_m1. QPCR reactions were run on QuantStudio 7 instrument. Relative quantification and fold changes were calculated using *dd*CT values against *Gapdh* and normalized to control-treated animals. For PDAC xenografts, RNA was isolated from tumor sections using Qiagen RNeasy kit (cat#74106), then cDNA was prepared using 2 μg of RNA and the high capacity RNA to cDNA kit (Applied Biosystems, cat#4387406) as per manufacturer's instructions. Biomarker expression was determined using Taqman gene expression probes (S1 Table)

and Universal master mix (ThermoFisher Scientific cat#4305719) with expression levels normalized to *Gapdh*.

For cytokine production, ears are removed, split in half using forceps and floated, dermis side-down, in DMEM media (Gibco) and incubated at 37°C for 24 hours. Following incubation, media was removed and cytokine production assessed by Luminex assay (Bio-Rad Laboratories).

Bioanalysis & pharmacokinetic measurements

In the IMQ-induced inflammation model, whole blood (300–500 μL) was collected and centrifuged (1000 g x 10 min) at 20°C to obtain plasma samples. In KP/C mouse model, tumors were collected and homogenized with phosphate buffer at ratio of 1:3 (w:v). Plasma standard curves were prepared by adding each test compound in to mouse plasma and serial diluting to desired concentration. Blank tumor homogenate and blank plasma was add to plasma standards and tumor homogenate samples, respectively, at 1:1 (v:v) ratio for matrix match of tumor sample analysis. An aliquot of 50 μL of each plasma sample, each tumor sample and each corresponding standards was added to 200 μL of acetonitrile with 100 ng/mL of carbutamide (Sigma Aldrich, St. Louis, MO), internal standard (IS), for protein precipitation, then filtered through a 96-well Orochem filtration plate (Orochem Technologies Inc., Naperville IL). Each extracted test compound in resultant supernatant was analyzed with appropriate liquid chromatography column eluting to a Sciex QTRAP 6500+ LC/MS/MS system (Applied Biosystems, Foster City, CA). Each analyte was characterized by Turbo IonSpray ionization multiple reaction monitoring (MRM). Quantitative drug concentrations were determined by standard calibration curve analysis, using linear fitting with $1/x^2$ weighted plot of the analyte/IS peak area ratio *vs* analyte concentration.

In vitro human Th17 cell differentiation & maintenance cultures

For differentiation assays, naïve CD4+ T cells were enriched (StemCell Technologies; 19555) from healthy donor human PBMCs and cultured in 96-well plates, with XVIV0-15 (Lonza; 04418Q) and anti-CD3/anti-CD28 Dynabeads (Thermo; 11161D). Th0 cell cultures were provided IL-2 (15 U/mL; R&D Systems 202-IL-500), while Th17 cell cultures were supplemented with IL-6 (20 ng/mL; R&D Systems 206-IL-010), TGF-β (10 ng/mL; R&D Systems 240-B002), IL-23 (10 ng/mL; R&D Systems 1290-IL-010) and IL-1β (10 ng/mL; R&D Systems; 201-LB-005). Compound or DMSO vehicle control was added on day 0, and on day 6 supernatants and cells were harvested for Luminex and flow cytometry, respectively. Supernatants were analyzed using a human Th17 cell cytokine panel multiplex (BioRad 171AA001M). For flow cytometry, cultured cells were incubated with phorbol 12-myristate 13-aetate (PMA) and ionomycin (eBioscience; 00-4333-57), in the presence of GolgiStop (BD; 554724) for 5 hours at 37°C. Single cell suspensions were stained with a fixable viability dye (Invitrogen; L34966) and intracellular staining for IL-17A (eBioscience; 50-7179-42; eBio64Dec17) and IFNγ (BD; 563563; b27) was performed as described in the Foxp3/Transcription Factor Staining Buffer kit (eBioscience; 00-5523-00). For Th17 cell maintenance cultures, Th17 cells were enriched (StemCell Technologies; 17862) from healthy donor human PBMCs and cultured in 96 well plates in IMDM supplemented with 10% FBS, penicillin (10 U/mL), streptomycin (10 μg/mL), glutamine (2 mM), and β-mercaptoethanol (55 μM) in the presence of anti-CD3/anti-CD28 Dynabeads (Thermo; 11161D). Th17 cell maintenance cultures were supplemented with IL-23 (50 μg/mL) and IL-1β (10 ng/mL). Compound or DMSO vehicle control was added on day 0, and on day 4 supernatants and cells were harvested for Luminex and flow cytometry, respectively, as described above.

Statistical analyses

Statistical significance was determined using GraphPad Prism 8 Student's *t*-test or one-way ANOVA with Tukey's multiple comparisons test as indicated. Data presented are mean ± SEM. A *P*-value equal to or less than 0.05 was considered to be statistically significant.

Results

Design, synthesis and characterization of RORγt allosteric inhibitors

Three RORγt allosteric inhibitors (Fig 1A), similar to previously described molecular architectures disclosed by Lycera (patent estate licensed to Celgene in 2017) and Merck [19], were designed, synthesized, and characterized in a suite of immunology and oncology assays. Design of these inhibitors was focused on an indazole core with aims of enhancing ligand efficiency, facilitating synthetic preparation, and improving physicochemical properties. As previously determined by protein X-ray crystallography, structural analogs of Compounds **1–3** bind to an allosteric site of RORγt [22]. Though crystal structures were not obtained for these molecules, molecular modeling suggests they replicate key interactions, orientation and overall fit in the allosteric binding pocket compared to previously reported allosteric antagonists (S1 Fig). Compound **3** emerged as a lead candidate based upon its favorable potency and selectivity (S2 and S3 Tables), coupled with a moderate oral exposure across species, synthetic accessibility, and physicochemical properties.

A fit for purpose route to access Compound **3** was developed, employing 12 total synthetic steps and a longest linear sequence of 7 steps from commercially available starting materials (Fig 1). Compound **3** was prepared in 3% yield from 2,6-difluorobenzaldehyde. Acylation of diaholindazole Intermediate 1 (Int-**1**) was followed by a Suzuki–Miyaura coupling with enone Int-**3** in good yield. Treatment of the lithium enolate of Int-**4** with Mander's reagent gave the keto ester Int-**5**, which was reduced under Noyori conditions to give alcohol Int-**6**. Hydrolysis afforded the acid Int-**7**, which was recrystallized with (R)-(+)-1phenylethylamine to provide stereo-enriched Int-**8** in a 33% yield and 99% purity. Treatment of the Int-**8** salt with citric acid delivered the final compound 3. Single molecule X-ray crystallographic analysis confirmed the stereochemical configuration of Compound **3** as (*R*,*R*) (Fig 2). Access to Compound **1** and Compound **2** was accomplished in similar fashion.

RORγt inhibitors attenuate human Th17 cell differentiation and maintenance

To profile these RORγt inhibitors in biologically-relevant assays, the impact of treatment with Compounds **1–3** on Th17 cell differentiation and maintenance was assessed *in vitro*. RORγt is the central transcriptional regulator of Th17 cell identity, promoting expression of key subset effectors, including the lineage defining cytokine IL-17A [23, 24]. Previous studies have shown, through genetic deletion or small molecule inhibition, that RORγt is crucial for the development of Th17 cells and contributes to the maintenance of Th17 cell function [23, 25–30]. Human naïve CD4$^+$ T cells were cultured under Th17 cell polarizing conditions in the presence of titrating doses of compounds (Fig 3A). All three RORγt inhibitors blocked IL-17A secretion in a dose dependent manner with approximately 95% maximal inhibition relative to DMSO vehicle control (Fig 3D). All compounds had single digit nanomolar IC$_{50}$'s (S4 Table), with no overt cytotoxicity (S2A and S2B Fig). Intracellular cytokine staining also showed near complete inhibition of Th17 cell polarization, with the percentage of IL-17A$^+$ cells returning to levels comparable to those measured in nonpolarizing Th0 cell conditions (Fig 3C). All three RORγt inhibitors were also profiled in human memory Th17 cell cultures, in the presence of
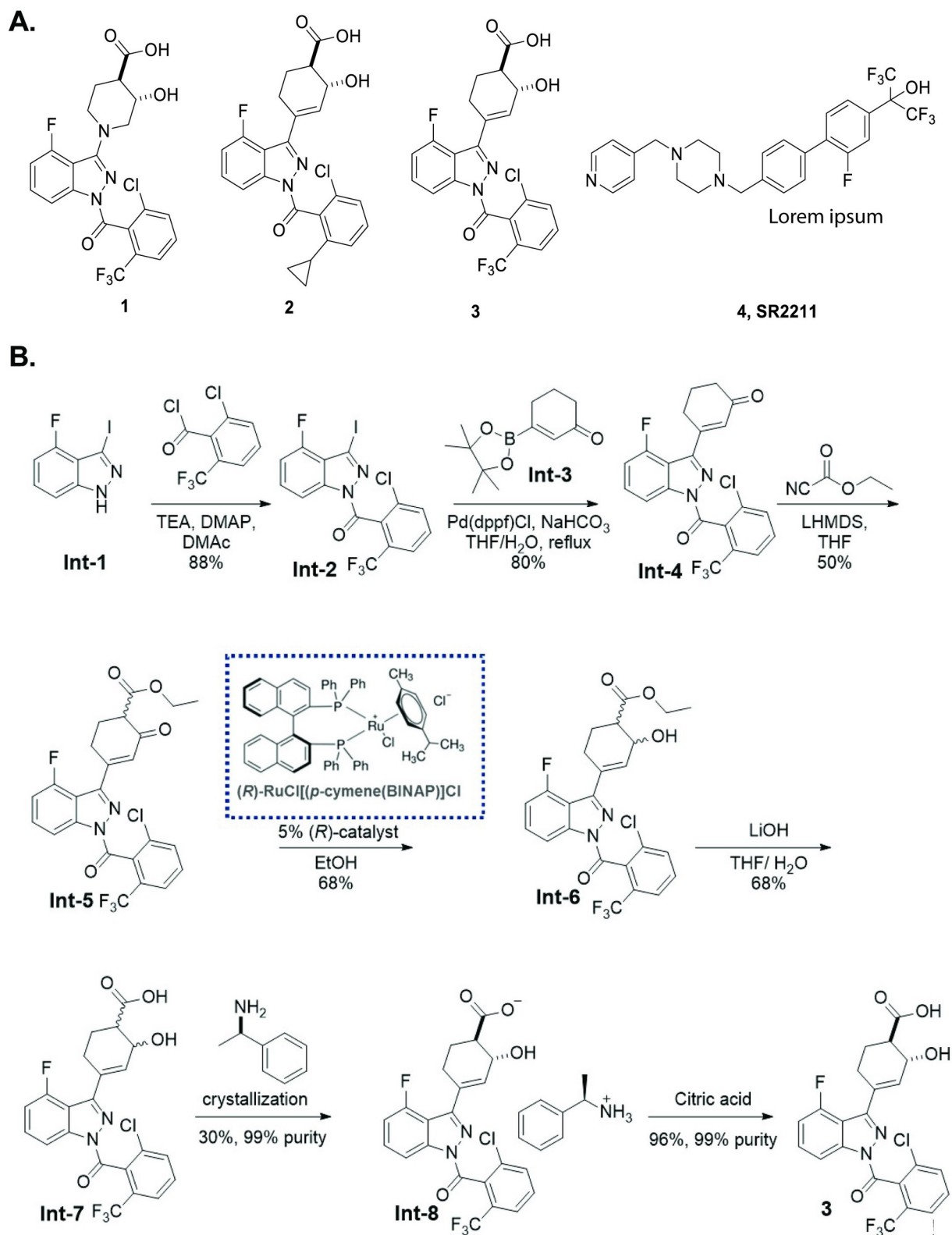
Fig 1. Representative RORγt inhibitors (Compounds 1–3) and inverse agonist, SR2211. Structures of Compounds **1–3** compared to inverse agonist, SR2211 (**A**) and chemical synthesis route for Compound **3** (**B**).
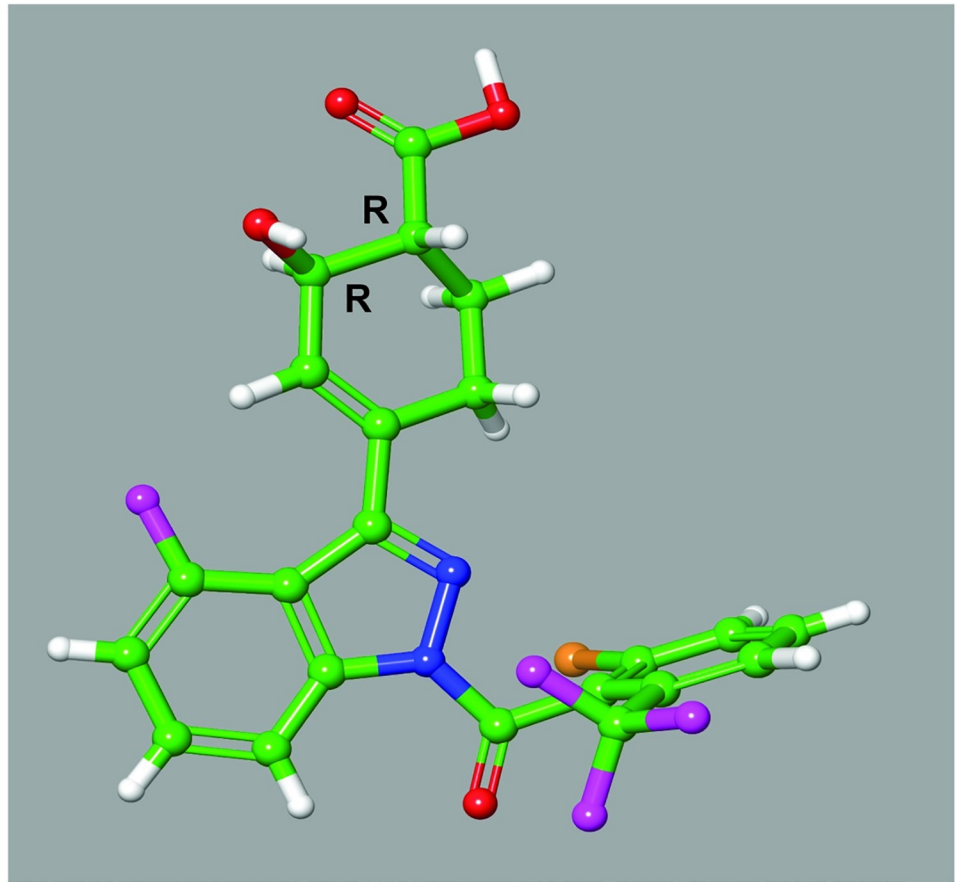
Fig 2. Single molecule X-ray crystallography of Compound 3. Small molecule X-ray structure of Compound **3** indicates only the (*R,R*)-enantiomer is present in the crystal structure. Crystal conformation of compound is and depicted in ball and stick representation (carbon–green; hydrogen–white; oxygen–red; nitrogen–blue; fluorine–magenta; chlorine–orange).

https://doi.org/10.1371/journal.pone.0248034.g002

lineage maintenance cytokines IL-23 and IL-1β (Fig 3B and 3E). Again, all compounds reduced IL-17A secretion in a dose dependent manner, with similar nanomolar IC_{50} values and no overt cytotoxicity (S4 Table and S2A and S2B Fig). Residual IL-17A production by memory Th17 cells is presumably attributable to amplification of the cytokine by additional transcription factors known to regulate its expression. Taken together, Compounds **1–3** resulted in inhibition of human Th17 cell differentiation and memory Th17 cell IL-17A production *in vitro*.

RORγt inhibitors attenuate imiquimod-induced skin inflammation & Th17-cytokine gene expression

To determine if IC_{50} vs IC_{90} coverage *in vivo* is required to significantly reduce IL-17-dependent gene expression, a 4-day model of Th17-dependent skin inflammation was developed by modifying the pre-clinical model of imiquimod (IMQ)-induced psoriasis. Topical administration of Aldara cream (5% IMQ) is a well-characterized model of Th17 cytokine-dependent skin inflammation [31–33] and a system in which RORγt inhibitors have been shown to attenuate inflammation [30]. Aldara cream was applied daily to the ears of Balb/c mice for 3 days, which were treated daily PO with vehicle or 30, 45 or 75 mg/kg of Compound **1**. On day 4, ear
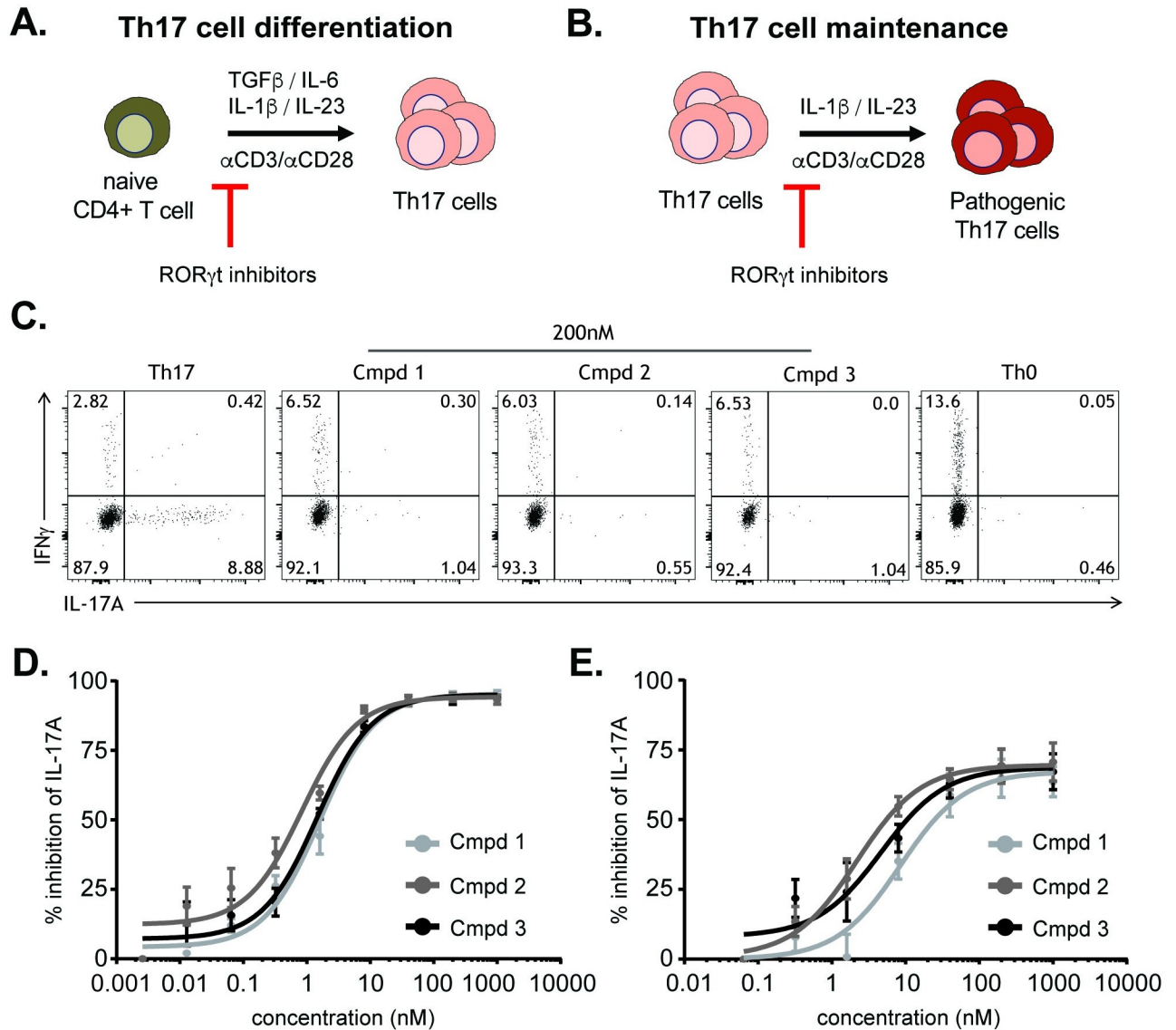
Fig 3. RORγt-mediated inhibition of IL-17A production in human Th17 cell cultures. Schematic of human Th17 differentiation (**A**) or Th17 maintenance (**B**) assays. Representative flow cytometry plots of intracellular cytokine staining from cultures from (A) including Th0 cell nonpolarizing condition (**C**). IL-17A cytokine production from enriched naïve CD4$^+$ T cells from healthy donor PBMC cultured under Th17 cell conditions for 6 days (**D**) or from enriched human Th17 cells from healthy donor PBMC cultured with IL-23 and IL-1β, for 4 days (**E**), in the presence of the indicated RORγt inhibitors Compounds **1–3**. Data are normalized to and represented as percent inhibition compared to DMSO controls. Error bars are representative of 4 individual donors, from 2 independent experiments.

https://doi.org/10.1371/journal.pone.0248034.g003

thickness was measured via calipers and then ears collected for either assessment of Th17-cytokine gene expression or cytokine production. As expected, IMQ-treated animals showed a significant thickening of the ear (0.21 ± 0.03 mm) compared to the control-treated group (0.15 ± 0.006 mm) (Fig 4A). In addition, RNA analysis from skin tissue of IMQ-treated animals demonstrated significantly increased expression of Th17-associated genes, *Il17a*, *Il17f* and *Il22* as well as IL-17A cytokine production (Fig 4B–4D and S3 Fig), compared to control treated animals. Compared to vehicle treated animals, Compound **1** significantly reduced ear thickening at doses of 45 and 75 mg/kg (0.17 ± 0.02 mm and 0.16 ± 0.008 mm, respectively) (Fig 4A), and reduced Th17-cytokine gene expression at all dose levels tested (Fig 4B–4D). To
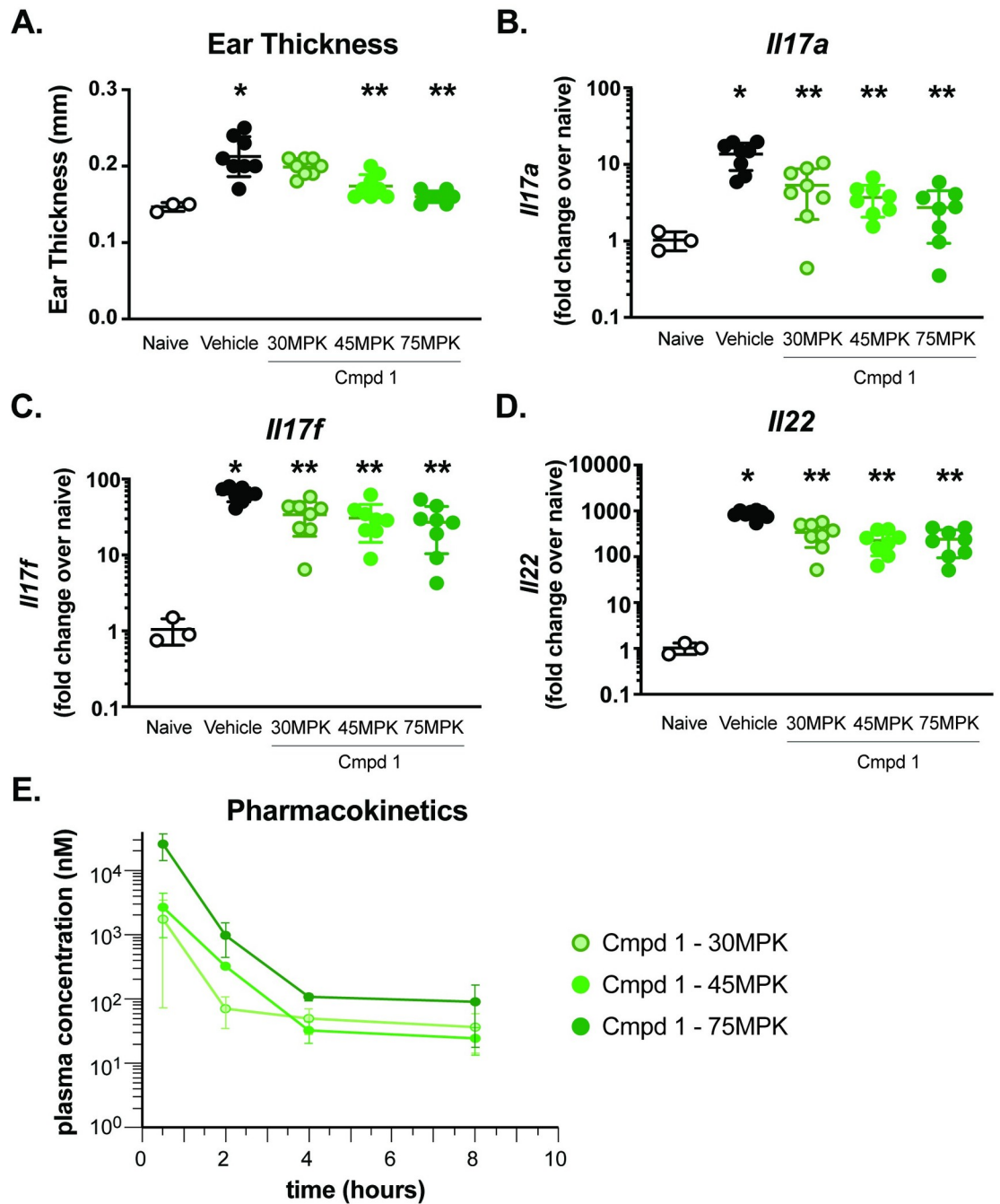
Fig 4. Imiquimod-induced skin inflammation is attenuated by RORγt inhibitor Compound 1. Ear thickness (mm) was measured in naïve or IMQ-treated animals on day 4 using digital micro-calipers (**A**). Th17 cytokine gene expression analysis was performed for *Il17a* (**B**), *Il17f* (**C**) and *Il22* (**D**) on day 4. Expression is normalized to *Gapdh* and presented as fold change over naïve. Kinetic assessment of plasma concentration of Compound **1** (**E**). Each symbol represents an individual animal and error bars denote mean ± SEM. Statistical significance ($^*p \leq 0.05$) was determined using one-way ANOVA with Tukey's multiple comparisons test, *significant over naïve; **significance over vehicle-treated group. Data are representative of 2 independent experiments with n = 3-8/group.

https://doi.org/10.1371/journal.pone.0248034.g004

determine PK/PD relationships, unbound murine IC_{50} and IC_{90} values were calculated based on murine and human GAL4 IC_{50}s (S2 Table) and human Th17 differentiation IC_{50} values and adjusted for murine plasma protein binding. Total plasma concentrations for Compound

1 of 108 nM and 975 nM correlate to free drug levels that cover IC_{50} and IC_{90}, respectively. Adjusted IC_{50} and IC_{90} plasma concentrations of 57 nM and 517 nM for Compound **2**, respectively, and concentrations of 116 nM and 1047 nM for Compound **3**, respectively, were determined. Plasma concentration of Compound **1** was monitored at 0.5, 2, 4 and 8 hours postdosing on day 4. The duration of free IC_{50} coverage in plasma, post PO doses of 30, 45 and 75 mg/kg, was 1.8, 2.9 and 3.9 hours, respectively (Fig 4E). In addition to attenuation of Th17-associated gene expression, treatment with Compound **1** also reduced IMQ-induced IL-17A cytokine production in ear tissues (S3 Fig).

Similar to Compound **1**, oral administration of indazole-containing RORγt inhibitors, Compound **2** and Compound **3,** resulted in decreased IMQ-induced skin inflammation. Administration of Compound **3** at 25, 50 or 100 mg/kg corresponded with unbound IC_{50} coverage (57 nM) of ~10, 12 and 18 hours and significantly reduced IMQ-induced ear thickening was observed at all doses (0.163 ± 0.002 mm, 0.156 ± 0.001 mm & 0.143 ± 0.002 mm at 25, 50 and 100 mg/kg respectively, compared to 0.17 ± 0.002 mm in control-treated mice). Th17-cytokine gene expression was reduced in the 50 and 100 mg/kg dosed groups (Fig 5A–5C). Attenuation of Th17 cytokine responses was observed with unbound IC_{50} coverage of ~18 hours in plasma, respectively (Fig 5E). Similarly, oral administration of Compound **2** resulted in inhibition of Th17-dependent gene expression and inflammation (S4 Fig). RORγt can also impact *Bclxl* expression in T cell populations, specifically in the thymus, leading to the development of lymphoma [34, 35], which represents a potential safety liability for this class of small molecules. Consistent with this, Compounds **1**, **2** and **3** resulted in modulation of *Bclxl* expression in the thymus (S5 Fig). To assess whether *Bclxl* expression and modulation could be detected following RORγt inhibition in tissues readily biopsied in a clinical setting without the need to collect thymic tissue (ie. skin), *Bclxl* expression was measured after oral administration of Compound **3** in the IMQ-induced skin inflammation. Similar to *Il17a* and *Il17f* expression, treatment with Compound **3** significantly reduced *Bclxl* expression in skin tissues (Fig 5D), suggesting that skin-specific *Bclxl* expression can be detected and changes in *Bclxl* expression in the skin could represent a biomarker with clinical utility.

To further assess the coverage required for inhibition of Th17-dependent skin inflammation, ratios of free drug concentrations in plasma and *Il17a* or *Il17f* expressions levels for individual animals were compared. As shown in Fig 6, the concentration of Compound **3** in plasma concentration inversely correlated with inhibition of Th17-associated *Il17a* (Fig 6A) and *Il17f* (Fig 6B) gene expression with r^2 = 0.37 and 0.44, respectively.

RORγt inhibitors reduce the severity of Th17-dependent inflammation in the central nervous system

We next sought to extend these findings to a chronic disease model where we could assess efficacy with prolonged compound exposure. To this end, an EAE model of IL-17-dependent CNS inflammation was employed. Following EAE induction, vehicle-treated animals showed significant disease starting at day 12 and reached a peak clinical score around day 26 of 3.08 ± 0.28 (Fig 7). As a positive control, FTY720 (3 mg/kg) significantly impacted disease onset (day 20) and severity (clinical score 0.54 ± 0.234). Treatment with Compound **3** at 3 or 10 mg/kg did not reduce EAE severity, with clinical scores of 2.79 ± 0.25 and 2.32 ± 0.21, respectively. However, Compound **3** dosed at 30 mg/kg significantly attenuated EAE severity (clinical score 1.5 ± 0.27) and delayed significant disease onset until day 15 (Fig 7). While not to the degree observed for the S1PR functional antagonist, FTY720, which blocks all lymphocyte migration out of lymphoid organs, these data demonstrate that inhibition of RORγt can provide efficacy in a disease relevant chronic inflammatory model and are consistent with the
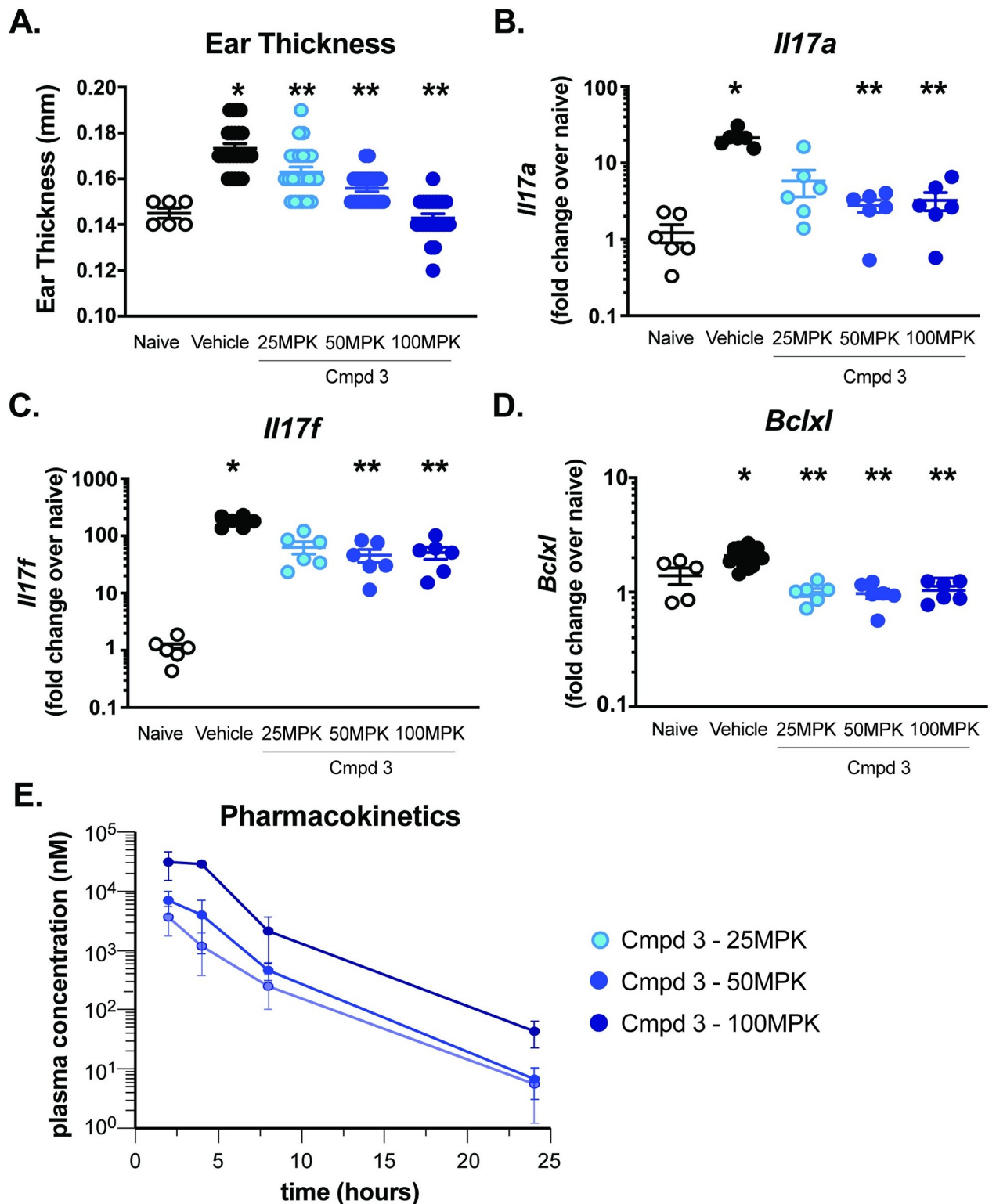
Fig 5. IMQ-induced skin inflammation and RORγt activity is inhibited by Compound 3. Ear thickness (mm) was measured in naïve or IMQ-treated animals on day 4 using digital micro-calipers (**A**). Th17 cytokine gene expression analysis was performed for *Il17a* (**B**), *Il17f* (**C**) and *Bclxl* (**D**) on day 4. Expression is normalized to *Gapdh* and presented as fold change over naïve. Kinetic assessment of plasma concentration of Compound **3** (**E**). Each symbol represents an individual animal and error bars denote mean ± SEM. Statistical significance (*$p \leq 0.05$) was determined using one-way ANOVA with Tukey's multiple comparisons test, *significant over naïve; **significance over vehicle-treated group. Data are representative of 1–4 independent experiments with n = 6-24/group.
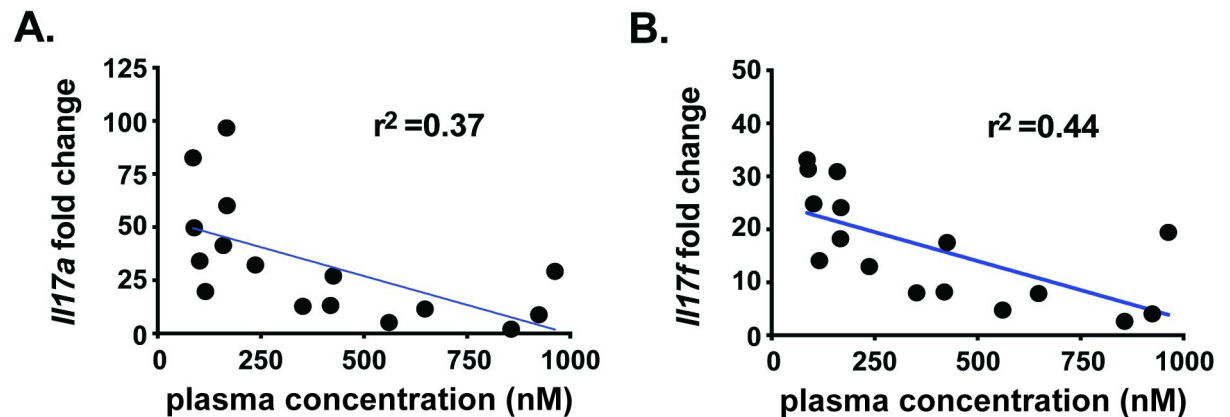
Fig 6. Compound 3 plasma concentration inversely correlates with Th17 cytokine gene expression. Th17 cytokine gene expression analysis was performed for *Il17a* (**A**) and *Il17f* (**B**) from IMQ-treated animals dosed with 6 or 60 mg/kg Compound **3**. Gene expression is normalized to *Gapdh* and presented as fold change over naïve and plotted relative to plasma concentrations for Compound **3**. Each symbol represents an individual animal and a linear regression (blue line) coefficient was calculated. Statistical significance (*$p \leq 0.05$) was determined using linear regression analysis. Data are from a single experiment with n = 8/group.

https://doi.org/10.1371/journal.pone.0248034.g006

observation that prolonged duration of IC_{50} coverage *in vivo* results in a more pronounced anti-inflammatory response.

RORγt antagonism and pancreatic organoid growth

A recent finding identified RORγt as a major regulator in human pancreatic stem cell growth and demonstrated that the pharmacologic inhibition of RORγt could reduce tumor burden in mouse models [16]. We, therefore sought to test the impact of Compound **3** as a therapeutic agent for treatment of pancreatic cancer. Patient-derived organoids (PDOs), which have been
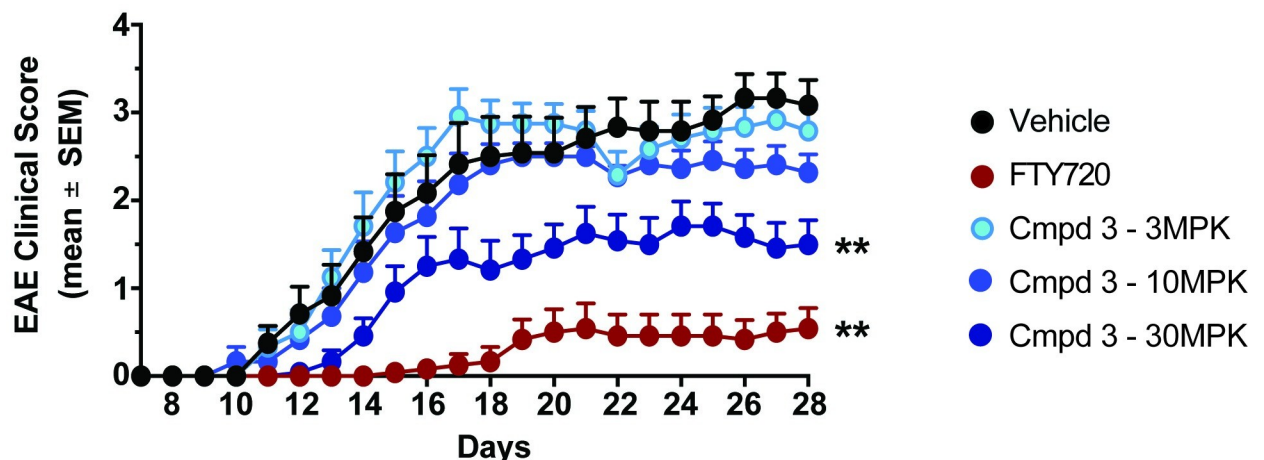
Fig 7. RORγt inhibitor protects in EAE immunization model. C57BL/6 mice were immunized with MOG$_{35-55}$ peptide on day 1 and were treated orally, twice daily (from day 1-day 28) with vehicle (0.5% MC/0.25% Tween80) or RORγt inhibitors at indicated doses. FTY720 (Gilenya) was dosed once daily at 3 mg/kg starting at day 1 in MilliQ water. The clinical score (0–5) was determined in these mice from day 7–28. Scores were calculated as follows: 0- no clinical signs, 0.5- partial tail weakness, 1.0- complete tail paralysis, 1.5- flaccid tail & abnormal gait, 2.0- flaccid tail and clear weakness of hind legs, 2.5- partial paralysis in one hind limb, 3.0- complete paralysis in both hindlimbs, 4.0- partial weakness in forelimbs, 5.0- complete paralysis in both forelimbs and hindlimbs). Data are presented as mean ± SEM. Statistical significance of clinical scores were calculated by Wilcoxon's non-parametric or 2-tailed Student's t-test, respectively; *$p < 0.05$, compared with vehicle-treated EAE mice. Data are from a single experiment with n = 12/group.

https://doi.org/10.1371/journal.pone.0248034.g007
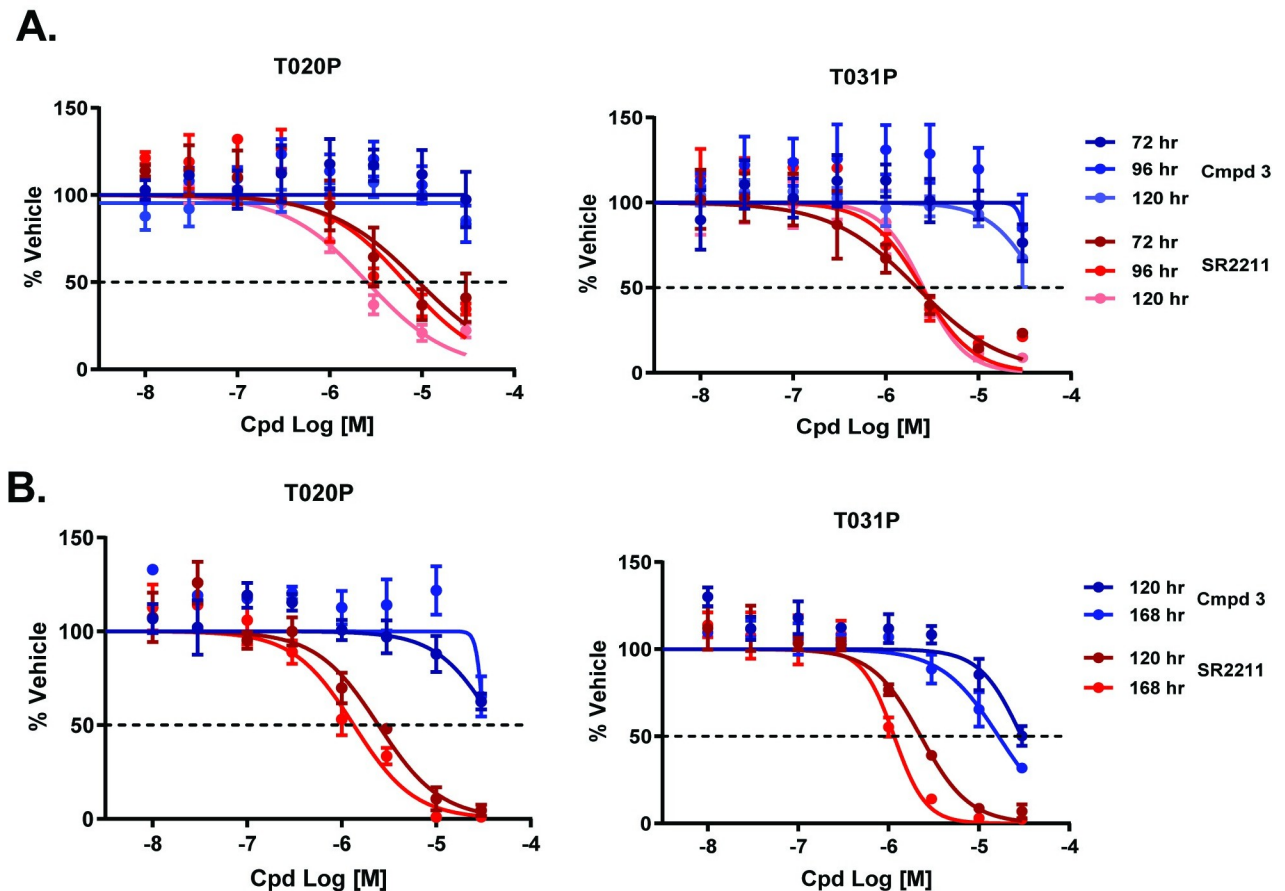
Fig 8. *In vitro* RORγt inhibitor activity on PDO growth & formation. PDOs T020P and T031P organoids were dissociated and treated with Compound **3** or SR2211 and either organoid growth or organoid formation defects examined. **(A)** Organoid growth assays, PDOs were treated with Compound **3** (red line) or SR2211 (blue line) beginning on day 3 after plating for the duration and dose indicated. All values were calculated as % relative to vehicle treated organoids in 3 replicate experiments. **(B)** Organoid formation assays, PDOs were treated with Compound **3** (red line) or SR2211 (blue line) starting on day 1 after plating for the duration and dose indicated. All values were calculated as % of vehicle treated organoids in 3 replicate experiments.

shown to effectively parallel patient responses to new therapeutic agents [36], were utilized to assay Compound **3** activity *in vitro*. The PDAC PDO model T020P was derived from a patient resistant to Abraxne, whereas the T031P model came from a treatment-naïve patient and was sensitive to Abraxane. To assess the effect of Compound 3 on organoid formation PDO cultures were treated 24 hr post-plating. Whereas to assess the effect of Compound **3** on organoid growth, PDO cultures were treated 3-days post-plating once organoid colonies had formed (S6 Fig). Organoid viability was assayed by Cell Titer Glo (CTG) at the time points indicated and compared with vehicle treated samples. The RORγt inhibitor SR2211 [37] inhibited the growth of both PDO models in a time and dose dependent manner with IC_{50} values ~3 µM. Contrary to this, Compound **3** decreased the growth of T031P ~30% at 30 µM after 120 hours of treatment but did not decrease viability of T020P PDOs (Fig 8A). To rule out drug instability as the reason for lack of efficacy of Compound **3** we repeated the experiment refreshing the compounds after 72 hr (S6 Fig). Re-treatment resulted in a slight increase in SR2211 activity but did not boost Compound 3 efficacy (S7A Fig). Compound **3** elicited a modest effect on organoid formation which increased in a time dependent manner for T031P with an IC_{50} of 30 µM at 120 hours and 10 µM at 168 hours. SR2211 demonstrated greater potency than Compound

3 with IC$_{50}$ values ~1 μM (Fig 8B) and in contrast to Compound **3**, a time dependent increase in activity for SR2211 was observed for all treatment intervals tested (Fig 8 and S7 Fig). Interestingly, the Abraxane resistant PDO model T020P was less sensitive to both compounds (Fig 8 and S7 Fig), suggesting a common resistance mechanism that may render RORγt inhibition less effective in patients pre-treated with Abraxane. In summary, the inverse agonist, SR2211, was more effective at inhibiting organoid growth than the allosteric inhibitor Compound **3**, suggesting that mode of modulation of RORγt is an important consideration. Despite their utility, PDO models do not fully recapitulate the heterogeneity and complexity of pancreatic cancer and tumor microenvironment signaling. Therefore, we sought to evaluate the antitumor activity of Compound **3** in a genetically engineered mouse model of pancreatic cancer.

Efficacy of Compound 3 in KP/C mouse model

To test whether inhibition of RORγt can lead to tumor growth inhibition we utilized the Kras$^{G12D/+}$/Trp53^{null}/Pdx1-cre (KP/C) mouse model of pancreatic cancer [20]. C57Bl/6 mice were inoculated in the flank with KP/C tumor chunks and enrolled in the study when the average tumor volume reached 200 mm^3. Efficacy of Compound **3** was evaluated either alone or in combination with gemcitabine and compared to either vehicle or cisplatin treated mice. As expected, gemcitabine and cisplatin significantly reduced the tumor volumes (Fig 9A). A trend towards reduced tumor size was observed after Compound 3 treatment, but the difference between vehicle and Compound 3 treated tumors was not statistically significant. Additionally, Compound **3** conferred no additional benefit when used in combination with gemcitabine (Fig 9A). At the conclusion of the study, tumors were harvested 16 hours post dosing and processed to determine intra-tumoral concentrations of Compound **3**. Tumor concentrations of Compound **3** were highly variable at 47 pmol/g ± 30 and 222 pmol/g ± 251 for Compound **3** as a single agent or in combination with gemcitabine, respectively (Fig 9B). Previous PK/PD analysis indicated that these concentrations are sufficient to achieve RORγt antagonism. To evaluate target engagement, we examined changes in expression of a subset of potential RORγt target genes in tumor samples. *Msi2* is proposed to be a marker of pancreatic cancer stem cells and a target gene of RORγt [16]. Interestingly, we observed a significant decrease in *Msi2* expression in tumors treated with a combination of Compound **3** and gemcitabine but not Compound **3** alone (Fig 9C). A similar pattern was observed for putative RORγt target genes *Ehf* and *Ncor2*. However, expression of other putative target genes, *Klf7* and *Osmr*, was decreased in all treatment groups (Fig 9C and S8 Fig). To summarize, modulation of a variety of RORγt target genes was achieved upon treatment with RORγt inhibitor Compound **3**, alone or in combination with standard of care agent gemcitabine. However, this activity was not sufficient to delay tumor volume in a KPC human tumor mouse model of pancreatic cancer.

Discussion

A multitude of pre-clinical data demonstrated that targeting the RORγt/IL-17A/IL-23 pathway ameliorates disease pathology in multiple autoimmune and inflammatory diseases. In addition, recent clinical successes of Otezla (Apremilast) and VTP-43742 (Vitae Pharmeuticals) in psoriasis, psoriatic arthritis, autoimmune uveitis and/or ankylosing spondylitis through reduction in circulating IL-17A levels [10, 11] support that targeting RORγt is a viable and potentially high value therapeutic strategy for IL-17-driven autoimmune disorders. Herein we report the design, synthesis and pre-clinical characterization of 3 potent, selective allosteric RORγt inhibitors (Compounds **1**, **2** and **3**) with structural similarity but also notable differences to those previously reported by Lycera and Merck [18, 19]. Compound **3** emerged as a lead candidate based upon its favorable potency and selectivity, as well as its cross-species
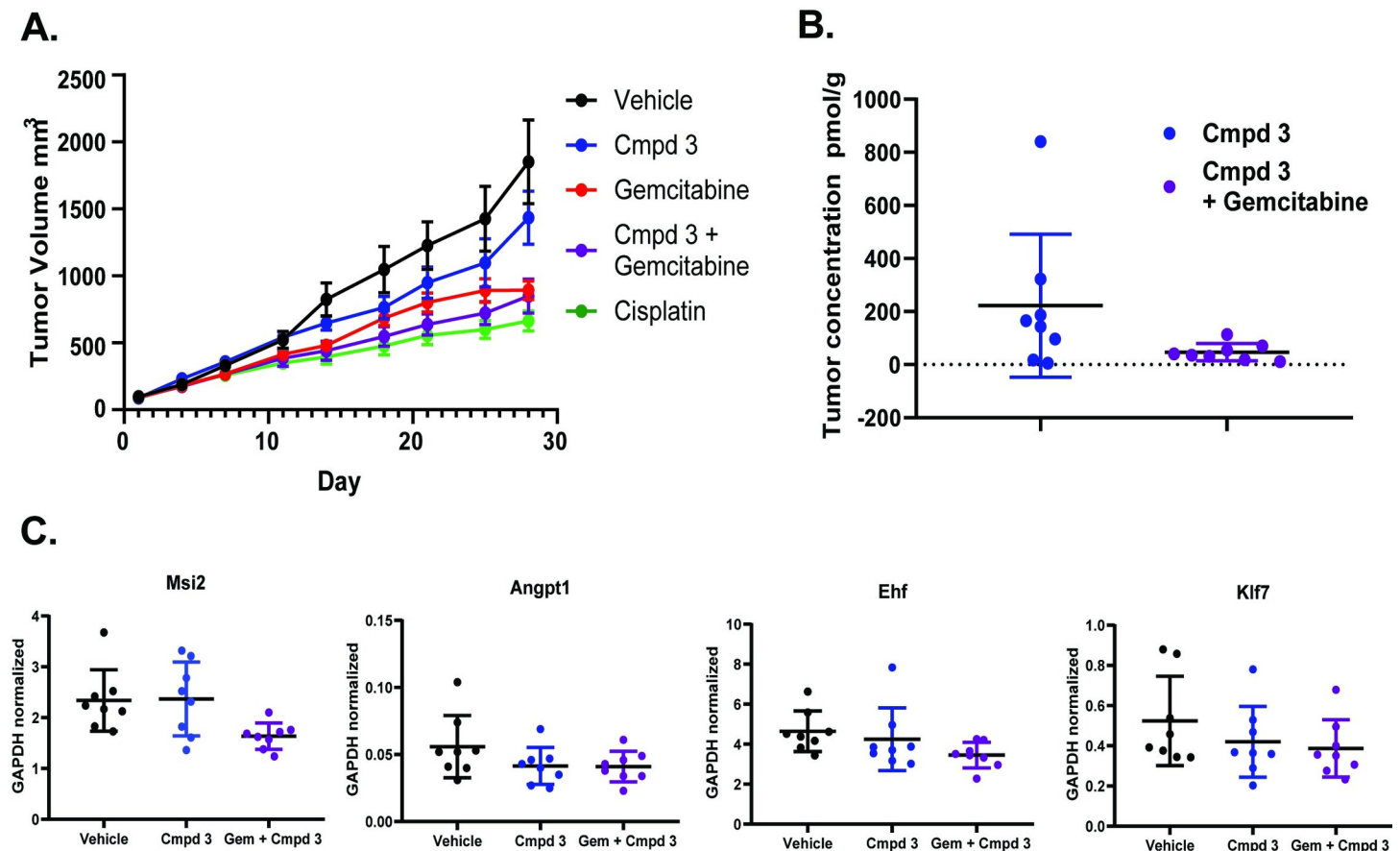
Fig 9. *In vivo* analysis of RORγt inhibitor activity on tumor growth. Tumors were implanted in the flanks of C57Bl/6 mice and treatment began when average tumor volume reached 200 mm^3. **(A)** Tumor volumes from animals treated with vehicle, Compound **3** alone, gemcitabine, Compound **3** plus gemcitabine or a positive control, cisplatin, were evaluated over 28 days of dosing. Averages were calculated from n = 8 mice per group. Error bars represent SEM. **(B)** Concentrations were measured by HPLC and plotted as mean ± SD. **(C)** qPCR expression analysis normalized to β-actin expression for vehicle, Compound **3**, or Compound **3** plus gemcitabine treated tumor samples and plotted as mean ± SD.

pharmacokinetic profile, synthetic accessibility and physicochemical properties. With a quality lead molecule in hand, we set out to interrogate the impact of allosteric inhibition of RORγt across models of immunology and oncology *in vitro* and *in vivo* systems.

RORγt is the central transcriptional regulator of γδT cells, group 3 innate lymphoid cell (ILC3), differentiating Th17 cells and memory Th17 cells [23, 24], promoting expression of key subset effectors, including the lineage defining cytokine IL-17A. Previous reports have demonstrated that RORγt-selective small molecule inhibitors can potently block pro-inflammatory IL-17A cytokine production in differentiating Th17 cells as well as in memory Th17 cells, whose expression of RORγt is pre-existing [27–30]. Consistent with these reports, the RORγt inhibitors Compounds **1–3** ablated Th17 cell differentiation and Th17 maintenance in human primary cells *in vitro*. Blockade of IL-17A secretion was achieved in a dose dependent manner with single digit nM IC_{50} concentrations, with no overt cell cytotoxicity. Interestingly, ~95% maximal inhibition with respect to Th17 differentiation corresponded to only ~60% inhibition in a Th17 maintenance assay. These data suggest that, within memory Th17 cells with pre-existing RORγt expression, a substantial fraction of the IL-17A production is independent of RORγt activity. As expected, the RORγt inhibitors did not have a significant impact on the frequency of cells producing the Th1 cell hallmark cytokine IFNγ, indicative of T helper lineage specificity.

In addition to potently inhibiting IL-17A responses in Th17 cells *in vitro*, we have demonstrated that allosteric RORγt inhibitors can ameliorate RORγt-dependent inflammation *in vivo*. Systemic administration of Compound **3** significantly reduced IMQ-induced ear thickening and Th17-cytokine gene expression. Further, treatment with Compound **3** significantly attenuated EAE severity, delayed disease onset and led to significant reductions in body weight loss that were maintained for the duration of study. Moreover, plasma concentrations of Compound **3** and *Il17a* or *Il17f* expression levels were inversely correlated with inhibition of Th17-associated gene expression. Importantly, attenuated IMQ-induced skin inflammation & EAE disease pathogenesis was only observed at doses that achieved IC_{50} coverage in excess of 18 hours, suggesting that extended time over IC_{50} is required for a durable response. Small molecule inhibition of RORγt resulted in ~75% inhibition of RORγt-dependent inflammation could be observed in both acute and chronic inflammatory model systems. It is important to note, that while, in our studies, Th17-associated gene expression was reduced overall at the tissue level, the specific impact of these RORγt inhibitors on distinct immune cell populations, ie ILC3, γδT cells, or, Th17 cells, was not assessed. While differential effects of these inhibitors would not be anticipated, the possibility remains that these different RORγt-dependent immune cell populations respond uniquely or differentially to RORγt allosteric inhibition. The functional and pathogenic implications of this, if true, as it relates to the cellular mechanisms of inflammatory diseases is an area of research that requires further investigation.

Pancreatic ductal adenocarcinoma, which accounts for ~95% of all pancreatic cancer cases, has a 5-year survival rate of only 8%. Surgical resection offers the best chance for increased survival, but only 20% of patients are diagnosed early enough to be candidates. Therefore, discovery of novel drivers and treatments for PDAC remains a high unmet need. A recent finding highlighted a potential role for RORγt in PDAC tumor growth and CSC maintenance [16]. RORγt inhibitors, which are currently under investigation in autoimmune and inflammatory diseases, could therefore represent a novel treatment mechanism for PDAC. The current study investigated efficacy of our RORγt allosteric inhibitor, Compound 3, in both *in vitro* and *in vivo* PDAC models. As expected, Compound **3** demonstrated greater inhibition of organoid formation compared to proliferation consistent with the proposed role for RORγt in CSC growth. In contrast, SR2211 demonstrated greater inhibition of organoid growth and formation suggesting that mode of inhibition may impact inhibitory potential. However off-target effects of SR2211 cannot be ruled out as differential activity was observed both *in vitro* and *in vivo*. Additionally, Compound **3** did not significantly reduce KP/C tumor growth and did not provide any additional benefit in combination with gemcitabine. RORγt inhibitors currently under investigation in autoimmune and inflammatory diseases may represent a novel treatment option for PDAC but further work is needed to determine a precise mechanism of action.

In this report we detailed the pre-clinical characterization of 3 selective and potent allosteric RORγt inhibitors and demonstrated inhibition of RORγt activity and subsequent RORγt-dependent inflammatory responses in multiple immune cells both *in vitro* and *in vivo*. A maximum of ~75% inhibition of RORγt-dependent inflammation was achieved in acute and chronic inflammatory settings. Interestingly, in our hands, VTP-43742, required extended IC_{90} coverage to achieve ~45% inhibition of Th17-dependent responses whereas Compound **3** achieved the same level of response with IC_{50} coverage alone. Given the clinical impact of VTP-43742 [11] and the proposed advantage of allosteric inhibition, Compound **3** may represent a complimentary treatment option for psoriasis.

There is a breadth of literature supporting a therapeutic benefit for targeting RORγt in Th17-driven autoimmune indications, however, there is also a potential safety liability in that knockout of RORγt in adult mice leads to development of lymphoblastic lymphomas within 6 months, in a manner similar to embryonic RORγt loss [14, 38]. Multiple reports have identified

RORγt inhibitors as causative agents in inducing lymphomas in rodents and non-human primates [34, 35]. Further, this effect is thought to be driven by RORγt mediated modulation of *Bclxl* expression in double negative (DN) T cell populations in the thymus, a phenomenon we observed in our studies. Human subjects with RORC knockout have been identified and do not exhibit signs of lymphoma [39], however, given our observations and additional reports of RORγt inhibition-induced thymocyte apoptosis in rodents & non-human primates (unpublished results: Bristol Myers Squibb (Haggerty et al. Society of Toxicology conference, 2020) and Genentech (Zbieg et al. Federation of Clinical Immunology Societies conference, 2018) the question remains whether the susceptibility to thymic lymphomas is a rodent-specific phenomenon and whether this presents a significant safety liability in human.

While the risk of lymphoma represents a significant hurdle for the development of RORγt inhibitors for the treatment of chronic autoimmune diseases, novel allosteric RORγt inhibitors reported herein may serve as additional tools for interrogation of RORγt biology. Decoupling of RORγt pathway inhibition and risk of thymic lymphomas, through suppression of Th17-mediated pathology, would represent a breakthrough with respect to the use of RORγt inhibitors for the treatment of autoimmune disorders, and would have the potential to provide a significant advancement in treatment options for patients worldwide.

Supporting information

S1 Table. QPCR primers.
(TIF)

S2 Table. IC$_{50}$ values for inhibition of human and murine RORγt. Concentrations of the RORγt inhibitors, Compound **1**, Compound **2** or Compound **3,** in which 50% (IC$_{50}$) relative light units (RLUs) was inhibited. Assays utilized reporter cells (HEK293) harboring a receptor hybrid in which the native N-terminal DNA binding domain (DBD) has been replaced with that of the yeast Gal4 DBD, with a firefly luciferase reporter gene functionally linked to a Gal4 upstream activation sequence.
(TIF)

S3 Table. Selectivity of human RORγt inhibitors. RORγt inhibitor selectivity of Compound **1**, Compound **2** or Compound **3** was assessed in nuclear hormone receptor binding assays, as measured by percent inhibition. Assays utilized reporter cells (HEK293) harboring a receptor hybrid in which the native N-terminal DNA binding domain (DBD) has been replaced with that of the yeast Gal4 DBD, with a firefly luciferase reporter gene functionally linked to a Gal4 upstream activation sequence. All compounds were dosed at 10 μM and percent inhibition calculated by relative light units (RLUs) compared to vehicle. *, repeat dose response curves failed to generate reliable IC50 values for compounds tested. RAR, RAR-related orphan receptor alpha; PPARγ, peroxisome proliferator-activated receptor gamma; TRα, thyroid hormone receptor alpha; GR, glucocorticoid receptor; LXR, liver X receptor.
(TIF)

S4 Table. RORγt inhibitors IC$_{50}$ values for inhibition of IL-17A production in human Th17 cell cultures. Concentrations of RORγt inhibitors Compound **1**, Compound **2** or Compound **3** in which 50% (IC$_{50}$) IL-17A cytokine was inhibited in Th17 differentiation or Th17 maintenance assays.
(TIF)

S1 Fig. Structural modeling of Compounds 1–3. Structural models of compounds **1–3** were built in RORγt structures (5C4T, 6UCG). The crystal structures were imported into Maestro

(Schrödinger Release 2020–2: Maestro, Glide, LigPrep, Epik, Schrödinger, LLC, New York, NY, 2020.). The structures were prepared using the Protein Preparation workflow as implemented in the Schrödinger Suite. Glide docking grids were generated by focusing the grid box on the center of the Cpd25 and MRL-673. The size of the box enclosing the grid was set to 10 Å. No other constraints, rotatable groups or excluded volumes were imposed. The three compounds **1–3** were then prepared for docking using LigPrep and the OPLS3e force field was used for minimizations; possible ionization states at pH 7.0 ± 2.0 were generated using Epik and tautomers were generated; specified chirality was retained.
(TIF)

S2 Fig. RORγt-mediated inhibition of IL-17A production in human Th17 cell cultures. Cell viability of enriched naïve CD4$^+$ T cells from healthy donor PBMC cultured under Th17 cell conditions, for 6 days (differentiation) **(A)** or enriched human Th17 cells from healthy donor PBMC cultured with IL-23 and IL-1β, for 4 days (maintenance) **(B)** in the presence of RORγt inhibitors Compound **1**, Compound 2 or Compound **3**. Data are normalized to and represented as percent of DMSO control. Error bars are representative of 4 individual donors, from 2 independent experiments.
(TIF)

S3 Fig. RORγt inhibitor inhibits IL-17A production in IMQ-treated ear tissue. IL-17A cytokine levels were measured by Luminex assay from the supernatants of ear tissue 'floats' cultured for 24 hours *ex vivo*. Each symbol represents an individual animal and error bars denote mean ± SEM. Statistical significance ($^*p \leq 0.05$) was determined using one-way ANOVA with Tukey's multiple comparisons test, *significant over naïve; **significance over vehicle-treated group. Data are representative of 2 independent experiments with n = 3-8/group.
(TIF)

S4 Fig. RORγt inhibitor Compound 2 reduces IMQ-induced Th17 cytokine-dependent inflammation. Ear thickness (mm) was measured in naïve or IMQ-treated animals on day 4 using digital micro-calipers **(A)**. Th17 cytokine gene expression analysis was performed for *Il17a* **(B)**, *Il17f* **(C)** and *Bclxl* **(D)** on day 4. Expression is normalized to *Gapdh* and presented as fold change over naïve. Each symbol represents an individual animal and error bars denote mean ± SEM. Statistical significance ($^*p \leq 0.05$) was determined using one-way ANOVA with Tukey's multiple comparisons test, *significant over naïve; **significance over vehicle-treated group. Data are representative of 2 independent experiments with n = 8/group.
(TIF)

S5 Fig. RORγt inhibitors reduce *Bclxl* expression in thymus of rodents. C57Bl/6 female mice were dosed PO with 100 mg/kg Compound **1**, **2** or **3**. Thymic tissues were collected from separate cohorts at 2, 8, 16 and 24 hours post-dose (n = 3 mice/timepoint). RNA was extracted from thymic tissues and *Bclxl* expression measured by QPCR. Data are normalized to housekeeping gene (*Gapdh*) and displayed as relative quantification. Time zero ('0') used as normalization timepoint and set to 1.0 RQ and mean set at 100% for % inhibition calculation. One-way ANOVA with Bonferroni correction for multiple comparisons used for statistical significance calculations.
(TIF)

S6 Fig. Schematic of Patient-derived organoids (PDO) growth & formation assays. PDOs were dissociated into single cells and plated on day 0. Organoids were treated beginning on day 1 or day 3 to assess effect on organoid formation or organoid growth, respectively. After

the indicated treatment schedule organoid growth or formation was assessed by CTG assay.
(TIF)

S7 Fig. *In vitro* RORγt inhibitor activity on PDO growth & formation. (A) PDOs were treated with Compound **3** or SR221 for 120 hours starting on day 1 after plating. PDOs were either subjected to a single treatment (NR) or compounds were replenished after 72 hours (RT). All values were calculated as % of vehicle treated organoids in 3 replicate experiments. **(B)** PDOs were treated with either Compound **3** or SR2211 for 72 or 120 hours starting on day 1 after plating. All values calculated as % vehicle treated organoids in 3 replicate experiments. **(C)** PDOs were treated for 120 hours with Compound **3** or SR2211 beginning on day 1 (D1) or day 3 (D3) post-plating. All values were calculated as % of vehicle treated organoids in 3 replicate experiments.
(TIF)

S8 Fig. Biomarker analysis from RORγt inhibitor treated tumors. qPCR expression analysis of indicated genes in vehicle, Compound **3** or Compound **3** plus Gemcitabine treated tumor samples. Replicate values plotted individually with mean ± SD represented.
(TIF)

Acknowledgments

Author Contributions

Conceptualization: Steven A. Saenz, Tiffany Carr, Lisa Beebe, Meghan Clements, J. Michael Ellis.

Data curation: Steven A. Saenz, Andrea Local, Tiffany Carr, Arvind Shakya, Shivsmriti Koul, Haiqing Hu, Lisa Chourb, Justin Stedman, Laura Akullian D'Agostino, Lisa Beebe, Meghan Clements, Laure Escoubet.

Formal analysis: Steven A. Saenz, Andrea Local, Tiffany Carr, Arvind Shakya, Shivsmriti Koul, Haiqing Hu, Lisa Chourb, Justin Stedman, Jenna Malley, Laura Akullian D'Agostino, John Malona, C. Eric Schwartz, Meghan Clements, Lan Jiang, Alex Dubrovskiy, Matt Kreilein, Roman Shimanovich.

Supervision: Laura Akullian D'Agostino, C. Eric Schwartz, Lisa Beebe, Ganesh Rajaraman, John Cho, Matt Kreilein, Roman Shimanovich, Lawrence G. Hamann, Laure Escoubet, J. Michael Ellis.

Visualization: Laura Akullian D'Agostino, Veerabahu Shanmugasundaram.

Writing – original draft: Steven A. Saenz, Andrea Local, Tiffany Carr, Laura Akullian D'Agostino, Laure Escoubet, J. Michael Ellis.

Writing – review & editing: Steven A. Saenz, Andrea Local.

References

1. Fitch E, Harper E, Skorcheva I, Kurtz SE, Blauvelt A. Pathophysiology of psoriasis: recent advances on IL-23 and Th17 cytokines. Curr Rheumatol Rep. 2007; 9(6):461–7. Epub 2008/01/08. https://doi.org/10.1007/s11926-007-0075-1 PMID: 18177599; PubMed Central PMCID: PMC2893221.

2. Lowes MA, Bowcock AM, Krueger JG. Pathogenesis and therapy of psoriasis. Nature. 2007; 445 (7130):866–73. Epub 2007/02/23. https://doi.org/10.1038/nature05663 PMID: 17314973.

3. Stockinger B, Veldhoen M. Differentiation and function of Th17 T cells. Curr Opin Immunol. 2007; 19 (3):281–6. Epub 2007/04/17. https://doi.org/10.1016/j.coi.2007.04.005 PMID: 17433650.

4. Kagami S, Rizzo HL, Lee JJ, Koguchi Y, Blauvelt A. Circulating Th17, Th22, and Th1 cells are increased in psoriasis. J Invest Dermatol. 2010; 130(5):1373–83. Epub 2009/12/25. https://doi.org/10.1038/jid.2009.399 PMID: 20032993; PubMed Central PMCID: PMC2892169.

5. Rutz S, Eidenschenk C, Kiefer JR, Ouyang W. Post-translational regulation of RORγt-A therapeutic target for the modulation of interleukin-17-mediated responses in autoimmune diseases. Cytokine Growth Factor Rev. 2016; 30:1–17. Epub 2016/08/03. https://doi.org/10.1016/j.cytogfr.2016.07.004 PMID: 27481185.

6. Kurebayashi S, Ueda E, Sakaue M, Patel DD, Medvedev A, Zhang F, et al. Retinoid-related orphan receptor gamma (RORgamma) is essential for lymphoid organogenesis and controls apoptosis during thymopoiesis. Proc Natl Acad Sci U S A. 2000; 97(18):10132–7. Epub 2000/08/30. https://doi.org/10.1073/pnas.97.18.10132 PMID: 10963675; PubMed Central PMCID: PMC27750.

7. Harrington LE, Hatton RD, Mangan PR, Turner H, Murphy TL, Murphy KM, et al. Interleukin 17-producing CD4+ effector T cells develop via a lineage distinct from the T helper type 1 and 2 lineages. Nat Immunol. 2005; 6(11):1123–32. Epub 2005/10/04. https://doi.org/10.1038/ni1254 PMID: 16200070.

8. Park H, Li Z, Yang XO, Chang SH, Nurieva R, Wang YH, et al. A distinct lineage of CD4 T cells regulates tissue inflammation by producing interleukin 17. Nat Immunol. 2005; 6(11):1133–41. Epub 2005/10/04. https://doi.org/10.1038/ni1261 PMID: 16200068; PubMed Central PMCID: PMC1618871.

9. Patel DD, Kuchroo VK. Th17 Cell Pathway in Human Immunity: Lessons from Genetics and Therapeutic Interventions. Immunity. 2015; 43(6):1040–51. Epub 2015/12/20. https://doi.org/10.1016/j.immuni.2015.12.003 PMID: 26682981.

10. Garcet S, Nograles K, Correa da Rosa J, Schafer PH, Krueger JG. Synergistic cytokine effects as apremilast response predictors in patients with psoriasis. J Allergy Clin Immunol. 2018; 142(3):1010–3.e6. Epub 2018/06/25. https://doi.org/10.1016/j.jaci.2018.05.039 PMID: 29936103.

11. Vitae Pharmaceuticals I. An Ascending Multiple Dose Study With VTP-43742 in Healthy Volunteers and Psoriatic Patients. ClinicalTrials.Gov: U.S. National Insitutes of Health: Bethesda, MD; 2016.

12. Bailey SR, Nelson MH, Himes RA, Li Z, Mehrotra S, Paulos CM. Th17 cells in cancer: the ultimate identity crisis. Front Immunol. 2014; 5:276. Epub 2014/07/06. https://doi.org/10.3389/fimmu.2014.00276 PMID: 24987392; PubMed Central PMCID: PMC4060300.

13. Zou W, Restifo NP. T(H)17 cells in tumour immunity and immunotherapy. Nat Rev Immunol. 2010; 10 (4):248–56. Epub 2010/03/26. https://doi.org/10.1038/nri2742 PMID: 20336152; PubMed Central PMCID: PMC3242804.

14. Liljevald M, Rehnberg M, Soderberg M, Ramnegard M, Borjesson J, Luciani D, et al. Retinoid-related orphan receptor gamma (RORgamma) adult induced knockout mice develop lymphoblastic lymphoma. Autoimmun Rev. 2016; 15(11):1062–70. Epub 2016/10/25. https://doi.org/10.1016/j.autrev.2016.07.036 PMID: 27491564.

15. Mahalingam D, Wang JS, Hamilton EP, Sarantopoulos J, Nemunaitis J, Weems G, et al. Phase 1 Open-Label, Multicenter Study of First-in-Class RORgamma Agonist LYC-55716 (Cintirorgon): Safety, Tolerability, and Preliminary Evidence of Antitumor Activity. Clin Cancer Res. 2019; 25(12):3508–16. Epub 2019/03/02. https://doi.org/10.1158/1078-0432.CCR-18-3185 PMID: 30819679.

16. Lytle NK, Ferguson LP, Rajbhandari N, Gilroy K, Fox RG, Deshpande A, et al. A Multiscale Map of the Stem Cell State in Pancreatic Adenocarcinoma. Cell. 2019; 177(3):572–86 e22. Epub 2019/04/09. https://doi.org/10.1016/j.cell.2019.03.010 PMID: 30955884; PubMed Central PMCID: PMC6711371.

17. Grosse-Wilde A, Fouquier d'Hérouël A, McIntosh E, Ertaylan G, Skupin A, Kuestner RE, et al. Stemness of the hybrid Epithelial/Mesenchymal State in Breast Cancer and Its Association with Poor Survival. PLoS One. 2015; 10(5):e0126522. Epub 2015/05/29. https://doi.org/10.1371/journal.pone.0126522 PMID: 26020648; PubMed Central PMCID: PMC4447403.

18. Scheepstra M, Leysen S, van Almen GC, Miller JR, Piesvaux J, Kutilek V, et al. Identification of an allosteric binding site for RORγt inhibition. Nat Commun. 2015; 6:8833. Epub 2015/12/08. https://doi.org/10.1038/ncomms9833 PMID: 26640126; PubMed Central PMCID: PMC4686831 S.N., S.M.S., M.K., K.W., N.E., M.v.d.S., J.R.M., J.P., V.K., H.v.E., G.P., S.S., A.O., B.W.T., and C.C.C. are current or previous employees of Merck & Co.

19. Zhang H, Lapointe BT, Anthony N, Azevedo R, Cals J, Correll CC, et al. Discovery of N-(Indazol-3-yl) piperidine-4-carboxylic Acids as RORγt Allosteric Inhibitors for Autoimmune Diseases. ACS Med Chem Lett. 2020; 11(2):114–9. Epub 2020/02/20. https://doi.org/10.1021/acsmedchemlett.9b00431 PMID: 32071676; PubMed Central PMCID: PMC7025379.

20. Hingorani SR, Wang L, Multani AS, Combs C, Deramaudt TB, Hruban RH, et al. Trp53R172H and KrasG12D cooperate to promote chromosomal instability and widely metastatic pancreatic ductal

adenocarcinoma in mice. Cancer Cell. 2005; 7(5):469–83. Epub 2005/05/17. https://doi.org/10.1016/j.ccr.2005.04.023 PMID: 15894267.

21. Boj SF, Hwang CI, Baker LA, Chio II, Engle DD, Corbo V, et al. Organoid models of human and mouse ductal pancreatic cancer. Cell. 2015; 160(1–2):324–38. Epub 2015/01/06. https://doi.org/10.1016/j.cell.2014.12.021 PMID: 25557080; PubMed Central PMCID: PMC4334572.

22. Zhang Y, Luo XY, Wu DH, Xu Y. ROR nuclear receptors: structures, related diseases, and drug discovery. Acta Pharmacol Sin. 2015; 36(1):71–87. Epub 2014/12/17. https://doi.org/10.1038/aps.2014.120 PMID: 25500868; PubMed Central PMCID: PMC4571318.

23. Korn T, Bettelli E, Oukka M, Kuchroo VK. IL-17 and Th17 Cells. Annu Rev Immunol. 2009; 27:485–517. Epub 2009/01/10. https://doi.org/10.1146/annurev.immunol.021908.132710 PMID: 19132915.

24. Cua DJ, Tato CM. Innate IL-17-producing cells: the sentinels of the immune system. Nat Rev Immunol. 2010; 10(7):479–89. Epub 2010/06/19. https://doi.org/10.1038/nri2800 PMID: 20559326.

25. Ivanov II, McKenzie BS, Zhou L, Tadokoro CE, Lepelley A, Lafaille JJ, et al. The orphan nuclear receptor RORgammat directs the differentiation program of proinflammatory IL-17+ T helper cells. Cell. 2006; 126(6):1121–33. Epub 2006/09/23. https://doi.org/10.1016/j.cell.2006.07.035 PMID: 16990136.

26. Manel N, Unutmaz D, Littman DR. The differentiation of human T(H)-17 cells requires transforming growth factor-beta and induction of the nuclear receptor RORgammat. Nat Immunol. 2008; 9(6):641–9. Epub 2008/05/06. https://doi.org/10.1038/ni.1610 PMID: 18454151; PubMed Central PMCID: PMC2597394.

27. Huh JR, Leung MW, Huang P, Ryan DA, Krout MR, Malapaka RR, et al. Digoxin and its derivatives suppress TH17 cell differentiation by antagonizing RORγt activity. Nature. 2011; 472(7344):486–90. Epub 2011/03/29. https://doi.org/10.1038/nature09978 PMID: 21441909; PubMed Central PMCID: PMC3172133.

28. Kumar N, Solt LA, Conkright JJ, Wang Y, Istrate MA, Busby SA, et al. The benzenesulfoamide T0901317 [N-(2,2,2-trifluoroethyl)-N-[4-[2,2,2-trifluoro-1-hydroxy-1-(trifluoromethyl)ethyl]phenyl]-benzenesulfonamide] is a novel retinoic acid receptor-related orphan receptor-alpha/gamma inverse agonist. Mol Pharmacol. 2010; 77(2):228–36. Epub 2009/11/06. https://doi.org/10.1124/mol.109.060905 PMID: 19887649; PubMed Central PMCID: PMC2812071.

29. Solt LA, Kumar N, Nuhant P, Wang Y, Lauer JL, Liu J, et al. Suppression of TH17 differentiation and autoimmunity by a synthetic ROR ligand. Nature. 2011; 472(7344):491–4. Epub 2011/04/19. https://doi.org/10.1038/nature10075 PMID: 21499262; PubMed Central PMCID: PMC3148894.

30. Banerjee D, Zhao L, Wu L, Palanichamy A, Ergun A, Peng L, et al. Small molecule mediated inhibition of RORγ-dependent gene expression and autoimmune disease pathology in vivo. Immunology. 2016; 147(4):399–413. Epub 2015/12/24. https://doi.org/10.1111/imm.12570 PMID: 26694902; PubMed Central PMCID: PMC4799885.

31. Cai Y, Shen X, Ding C, Qi C, Li K, Li X, et al. Pivotal role of dermal IL-17-producing γδ T cells in skin inflammation. Immunity. 2011; 35(4):596–610. Epub 2011/10/11. https://doi.org/10.1016/j.immuni.2011.08.001 PMID: 21982596; PubMed Central PMCID: PMC3205267.

32. Mabuchi T, Takekoshi T, Hwang ST. Epidermal CCR6+ γδ T cells are major producers of IL-22 and IL-17 in a murine model of psoriasiform dermatitis. J Immunol. 2011; 187(10):5026–31. Epub 2011/10/11. https://doi.org/10.4049/jimmunol.1101817 PMID: 21984702.

33. Pantelyushin S, Haak S, Ingold B, Kulig P, Heppner FL, Navarini AA, et al. Rorγt+ innate lymphocytes and γδ T cells initiate psoriasiform plaque formation in mice. J Clin Invest. 2012; 122(6):2252–6. Epub 2012/05/02. https://doi.org/10.1172/JCI61862 PMID: 22546855; PubMed Central PMCID: PMC3366412.

34. Guntermann C, Piaia A, Hamel ML, Theil D, Rubic-Schneider T, Del Rio-Espinola A, et al. Retinoic-acid-orphan-receptor-C inhibition suppresses Th17 cells and induces thymic aberrations. JCI Insight. 2017; 2(5):e91127. Epub 2017/03/16. https://doi.org/10.1172/jci.insight.91127 PMID: 28289717; PubMed Central PMCID: PMC5333964 Novartis. ADRE works for Novartis. All other authors work for and own shares or options of Novartis.

35. Guo Y, MacIsaac KD, Chen Y, Miller RJ, Jain R, Joyce-Shaikh B, et al. Inhibition of RORγT Skews TCRα Gene Rearrangement and Limits T Cell Repertoire Diversity. Cell Rep. 2016; 17(12):3206–18. Epub 2016/12/24. https://doi.org/10.1016/j.celrep.2016.11.073 PMID: 28009290.

36. Driehuis E, van Hoeck A, Moore K, Kolders S, Francies HE, Gulersonmez MC, et al. Pancreatic cancer organoids recapitulate disease and allow personalized drug screening. Proc Natl Acad Sci U S A. 2019; 116(52):26580–90. Epub 2019/12/11. https://doi.org/10.1073/pnas.1911273116 PMID: 31818951; PubMed Central PMCID: PMC6936689.

37. Kumar N, Lyda B, Chang MR, Lauer JL, Solt LA, Burris TP, et al. Identification of SR2211: a potent synthetic RORγ-selective modulator. ACS Chem Biol. 2012; 7(4):672–7. Epub 2012/02/02. https://doi.org/10.1021/cb200496y PMID: 22292739; PubMed Central PMCID: PMC3331898.

38. Ueda E, Kurebayashi S, Sakaue M, Backlund M, Koller B, Jetten AM. High incidence of T-cell lymphomas in mice deficient in the retinoid-related orphan receptor RORgamma. Cancer Res. 2002; 62 (3):901–9. Epub 2002/02/07. PMID: 11830550.

39. Okada S, Markle JG, Deenick EK, Mele F, Averbuch D, Lagos M, et al. IMMUNODEFICIENCIES. Impairment of immunity to Candida and Mycobacterium in humans with bi-allelic RORC mutations. Science. 2015; 349(6248):606–13. Epub 2015/07/15. https://doi.org/10.1126/science.aaa4282 PMID: 26160376; PubMed Central PMCID: PMC4668938.